Ca-substituted P3-type NaxNi1/3Mn1/3Co1/302 as a potential high voltage cathode active material for sodium-ion batteries

Matsui, Masaki
Mizukoshi, Fumikazu
Hasegawa, Hirona
Imanishi, Nobuyuki

(Citation)
Journal of Power Sources,485:229346

(Issue Date)
2021-02-15

(Resource Type)
journal article

(Version)
Accepted Manuscript

(URL)
https://hdl.handle.net/20.500.14094/90007834

Ca-substituted P3-type $Na_xNi_{1/3}Mn_{1/3}Co_{1/3}O_2$ as a Potential High Voltage Cathode Active Material for Sodium-ion Batteries

Masaki Matsui[1,2*], Fumikazu Mizukoshi[3], Hirona Hasegawa[1] and Nobuyuki Imanishi[2, 3]

1. Department of Chemical Science and Engineering, Kobe University
   1-1 Rokkodai-cho, Nada-ku, Kobe, 657-8501, Hyogo, JAPAN

2. Elements Strategy Initiative for Catalyst and Batteries (ESICB), Kyoto University
   1-30 Goryo Ohara, Nishikyo-ku, Kyoto, 615-8524, Kyoto, JAPAN

3. Department of Chemistry, Mie University
   1-31 1577 Kurimamachiya-cho, Tsu, 514-8507, Mie, JAPAN

Corresponding Author: Masaki Matsui
Affiliation: Department of Chemical Science and Engineering, Kobe University
phone & fax: +81-78-803-6160
e-mail: matsui@godzilla.kobe-u.ac.jp

ABSTRACT

The electrochemical property of the layered sodium transition metal oxide is dependent upon the reversible phase transition during the sodium intercalation/deintercalation process. Here we synthesized Ca-doped P3-type $Na_xNi_{1/3}Mn_{1/3}Co_{1/3}O_2$ as a potential cathode active material for sodium-ion batteries. The Ca-doping leads the lattice expansion along the c-axis, due to the electrostatic repulsion between Ca^{2+} ions and the transition metal ions. Even though the doped Ca^{2+} ions occupy Na^+ sites, the Ca-doped cathode shows lower overpotential during the galvanostatic charge-discharge process. The electrochemical impedance spectroscopy proved that the charge-transfer resistance of the Ca-doped layered oxide is lower than the Ca-free one at low cell voltage. These results indicate that the Ca-doping enhances the mobility of the Na^+ ions in the layered structure. The doped Ca^{2+} ions also suppress the irreversible O'3–O1 phase transition upon the full deintercalation of the sodium ions from the layered structure. The improved stability of the Ca-doped $Na_xNi_{1/3}Mn_{1/3}Co_{1/3}O_2$ leads better capacity retention during the galvanostatic cycling.

KEYWORDS

sodium ion batteries, intercalation, layered transition metal oxide, phase transition, reversibility

INTRODUCTION

Lithium-ion batteries (LIBs) power almost all the portable electronics such as smartphones, laptops, tablets, and digicams. The demands for LIBs are even increasing in large-format cells due to the development of electric vehicles and grid storages for renewable energies. Since the limited lithium resources, however, is a critical issue for the continuous production of the batteries, other systems are widely explored in the last decade. Sodium-ion batteries (SIBs) are the most promising alternatives of the LIBs, due to material abundance and energy densities.

Layered sodium transition metal oxides Na_xMeO_2 (Me=transition metals) have been widely studied as candidates for the cathode active materials of SIBs[1].

The Na_xMeO_2 typically have edge-sharing MO_6 octahedral units forming MO_2 slabs stacked to build up the layered structure. The coordination environments: octahedral (O), tetrahedral (T), and prismatic (P), of the sodium ions, between the MO_2 slabs, determine the possible stacking sequences of the Na_xMO_2[2]. The O3-type Na_xMO_2 generally shows phase transition upon sodium extraction. The reversibility of the Na_xMO_2 is typically dependent on the transition metal oxide layer[3-16]. For example, O3-type $NaCoO_2$ shows good reversibility with O3-O'3 and O'3-P3 phase transitions, while O3-type $NaFeO_2$ shows poor reversibility upon phase transition, due to the migration of Fe^{3+} ions[17]. Moreover, the O3-type $NaFe_{0.5}Co_{0.5}O_2$ shows improved reversible capacity compared with both the $NaFeO_2$ and $NaCoO_2$[18]. It suggests the partial substitution of the transition metal suppresses the irreversible phase transition. Various combinations of transition metals are also investigated to improve the reversibility of the O3-type layered transition metal oxides[19-29]. O3-type $NaNi_{1/3}Mn_{1/3}Co_{1/3}O_2$ shows highly reversible phase transitions: O3-O'3, O'3-P3, and P3-P'3 during the sodium extraction process[30]. Hwang et al. synthesized Ni-rich core and Mn-rich shell structure for the improvement of the cycling performance and thermal stability[31]. These studies show that the structural stability upon the phase transition is crucial for the cycling performance.

We previously reported an alternate materials design strategy for the improvement of the cycling performance. We substituted the sodium ions in P2-type Na_xCoO_2 with divalent calcium ion to minimize the glide of the MO_2 slab, which induces the phase transition[32]. Even though the Ca-substituted P2-type Na_xCoO_2 successfully showed an improved cycling performance, the specific capacity was decreased, and the overpotential of the cell was increased as the trade-off. Structural refinement results suggested that the calcium substitution shrink the lattice constant along the c-axis. It is because the substituted Ca^{2+} ions mainly occupy the 2d prismatic site, which has six edge-sharing MO_6 octahedral units, to minimize the electrostatic repulsion between the calcium and transition metal ions. Our recent report proves that the Ca-substituted P3-type Na_xCoO_2 shows the improved cycling performance without the trade-off of the increased overpotential, because the migration barrier of the Na^+ ion is decreased[33]. Sun et al. also reported that the Ca-substituted O3-type layered cathode: $NaNi_{1/3}Fe_{1/3}Mn_{1/3}O_2$ showed improved cycling performance[34]. These studies suggest that the irreversible phase transitions during

the charge-discharge process are suppressed by the Ca-substitution. Also, the operation voltage ranges of the layered cathodes are only limited < 4.0 V among all the works above.

Here we developed P3-type $Na_{0.6-x}Ca_xNi_{1/3}Mn_{1/3}Co_{1/3}O_2$ as a potential high voltage cathode for the SIBs. The XRD study reveals that the substituted Ca^{2+} ions prevent the phase transition at the high electrode potential >4.0 V. Also, the electrochemical impedance spectroscopy proves that the NCNMCO has lower charge-transfer resistance compared with NNMCO. Our results show an opportunity for further improvement in the energy density of SIBs.

EXPERIMENTAL

The NNMCO and NCNMCO were prepared by conventional solid-state methods using a stoichiometric amount of sodium hydroxide (NaOH, Wako), and nickel-manganese-cobalt mixed hydroxide ($Ni_{1/3}Mn_{1/3}Co_{1/3}(OH)_2$) and calcium hydroxide ($Ca(OH)_2$, Wako) as precursors. The excess NaOH of 5 wt.% was added to compensate for the evaporation of sodium during the calcination process. The $Ni_{1/3}Mn_{1/3}Co_{1/3}(OH)_2$ is prepared by the co-precipitation method using a mixed transition metal sulfate solution and NaOH solution. The starting materials were thoroughly mixed using an agate motor and pestle in an Ar-filled glove box. The mixed precursors are calcined at 350 ºC for 36 hours in O_2 atmosphere. Characterization of the NNMCO and NCNMCO ware performed using an X-ray diffractometer (RINT 2500, Rigaku Japan) equipped with Cu-Kα radiation. The lattice constants of the specimen were calculated by the Pawley method using TOPAS-Academic Ver. 4.2. The crystal structural model was developed using a software VESTA[35]. The surface morphologies were observed using SEM (S4800, Hitachi Japan, JSM-6335F, JEOL Japan) and the elemental mapping was taken by EDX. The elemental analyses were also carried out using ICP-AES (Horiba Jobin Yvon ULTIMA 2000).

The electrochemical properties of the NNMCO and NCNMCO were studied using two-electrode cells (TJ-AC, Tomcell JAPAN). The composite electrodes were prepared by mixing 80: 10: 10 weight ratio of the active material, acetylene black (SuperP ®, Imerys France), and PVdF-HFP (KYNAR®, ARKEMA) dissolved in anhydrous N-Methyl-2-pyrrolidone (NMP, Aldrich US) for the preparation of the electrode slurry. The slurry was coated on an aluminum current collector, and the NMP was vacuum dried at 80 ºC. The dried electrode was punched into a circular disc of 16 mm diameter. The punched electrode was pressed at 10 MPa and dried at 120 ºC under vacuum. The loading level of the active material was approximately 6 mg cm^{-2}.

The obtained electrode was coupled with a sodium metal (Wako, JAPAN) electrode to prepare a half-cell. The electrolyte solution was 1 mol L^{-1} of $NaPF_6$ in ethylene carbonate (EC) and diethyl carbonate (DEC) mixed solvent (1:1 by volume), containing fluoroethylene carbonate (FEC) of 3 wt% as an electrolyte additive (Kishida, JAPAN). The galvanostatic charge-discharge tests were performed using a battery charger (BTS2004H, Nagano JAPAN). A potentio-galvanostat (Model 1253A, Solartron UK) with a frequency response analyzer (Model 1260A, Solartron, UK) was employed for the electrochemical impedance spectroscopy.

RESULT AND DISCUSSIONS

During the initial attempt to synthesize the NNMCO, the nickel oxide (NiO) impurity phase was formed under various synthesis conditions, as shown in Figure S1. The NiO formation is corresponding to the phase separation of the transition metal oxide at the calcination process. The transition metals in the P3-type layered oxides partially oxidized to tetravalent. Hence the calcination process needs to be carried out under a highly oxidizing atmosphere. In addition, the calcination process should be performed at low temperature because of the continuous evaporation of the sodium also initiates the phase separation. The optimized calcination condition for the P3-type NNMCO is 350 ºC for 36 hours under pure oxygen flow.

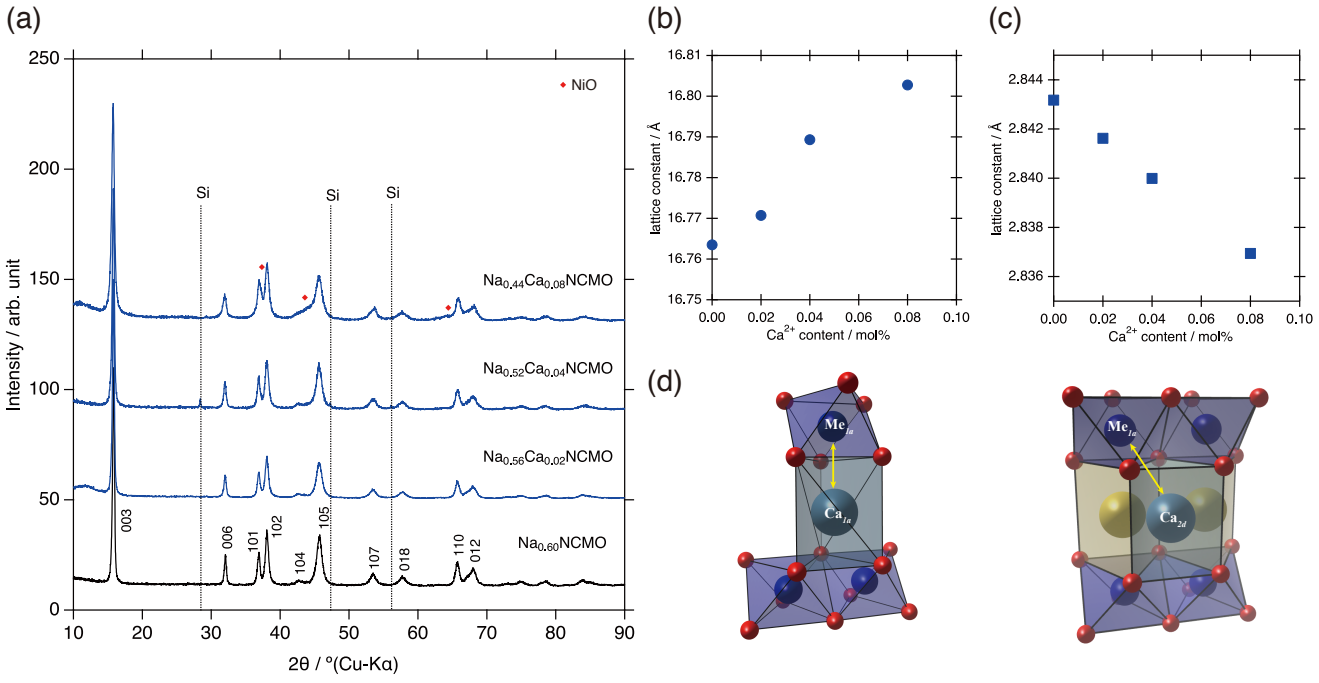

Figure. 1 X-ray diffraction patterns of the calcium substituted P3-type $Na_{0.6-2x}Ca_xNi_{1/3}Mn_{1/3}Co_{1/3}O_2$ (x=0, 0.02, 0.04, 0.08). The Ca-substitution expands the lattice along c-axis (b) and shrinks along a-axis (c). Comparison of the Ca^{2+}–Me distance between P3-type (left) and P2-type (right) layered structures (d).

Both the $Na_{0.6}$NMCO and $Na_{0.52}Ca_{0.04}$NMCO show the particle size of 5-10 μm as shown in Figure S2. The surface morphologies of these materials reflect the particle size of the precursor: the $Ni_{1/3}Mn_{1/3}Co_{1/3}(OH)_2$ mixed hydroxide particles. Figure 1 (a) shows XRD patterns of the NCNMCO, synthesized with various Ca^{2+} contents. The $Na_{0.6-2x}Ca_x$NMCO containing Ca^{2+} 0.02 and 0.04 show P3-type single phases, while the $Na_{0.44}Ca_{0.08}$NMCO contains NiO as the impurity phase, as shown in Figure 1 (a). The formation of the NiO at the high Ca content is due to the relatively slow diffusion of the Ca^{2+} ions during the solid-state reaction. The NaOH and $Ni_{1/3}Mn_{1/3}Co_{1/3}(OH)_2$ initially form the Na deficient layered oxide, before the incorporation of the Ca^{2+} ions into the layered structure. Since the low Na content requires highly oxidative state of transition metals, nickel is easily kicked out from the layered structure because the nickel preferably takes divalent, while manganese and cobalt prefer tetravalent and trivalent, respectively. The lattice constants along c-axis and a-axis are shown in Figure 1 (b) and (c), respectively. The trend of the lattice expansion/shrinkage by Ca-doping is opposite to the P2 type layered oxide in our previous paper. In the case of P3 type layered oxides, the 1a prismatic site has a face-sharing MeO_6 octahedron and three edge-sharing MeO_6 octahedra. Therefore, the substituted Ca^{2+} ion always has a transition metal ion at the face-sharing octahedron, as shown in Figure 1 (d). We consider that the electrostatic repulsion between the Ca^{2+} ion and the transition metal ion expand the lattice along the c-axis because of the relatively small Ca–Me distance in the P3 structure. On the other hand, the P2-type structure has two of the prismatic sites: 2b and 2d sites, for the Ca^{2+} ions. The Ca^{2+} ions preferably occupy the 2d sites because the 2b sites have two of the face-sharing MeO_6 octahedra, which cause relatively high electrostatic repulsion forces. Hence, the neighboring Ca–Me distance becomes approximately 13 % longer, and leads 22 % lower electrostatic repulsion force. Also, we suspect the relatively weak repulsion force leads to shrinkage of the lattice.

Figure 2 shows typical charge-discharge profiles of the P3 type layered NNMCO compared with NCNMCO in the voltage range of 1.3-4.2 V. The NNMCO shows a discharging capacity of 165.4 mAh g^{-1} while the charging capacity is 177.6 mAh g^{-1}. The coulombic efficiency of 93.1 % suggests two possible degradation processes: irreversible phase transition at the high electrode potential and oxidation of the electrolyte solution are occurring during the charging/discharging process. On the other hand, the NCNMCO shows significant improvement in reversibility. The $Na_{0.56}Ca_{0.02}$NMCO and $Na_{0.52}Ca_{0.04}$NMCO show the coulombic efficiency of 96.8 % and 99.5 % respectively. Since the doped Ca^{2+} ions replace the Na^{+} ions in the layered oxide, the specific capacity slightly decreases by the Ca-doping. The $Na_{0.52}Ca_{0.04}$NMCO shows a higher reversible capacity than $Na_{0.56}Ca_{0.02}$NMCO because of the improved coulombic efficiency of > 99 %. The improved reversibility of $Na_{0.52}Ca_{0.04}$NMCO suggests that the Ca^{2+} doping suppresses the irreversible phase transition during the charging/discharging process.

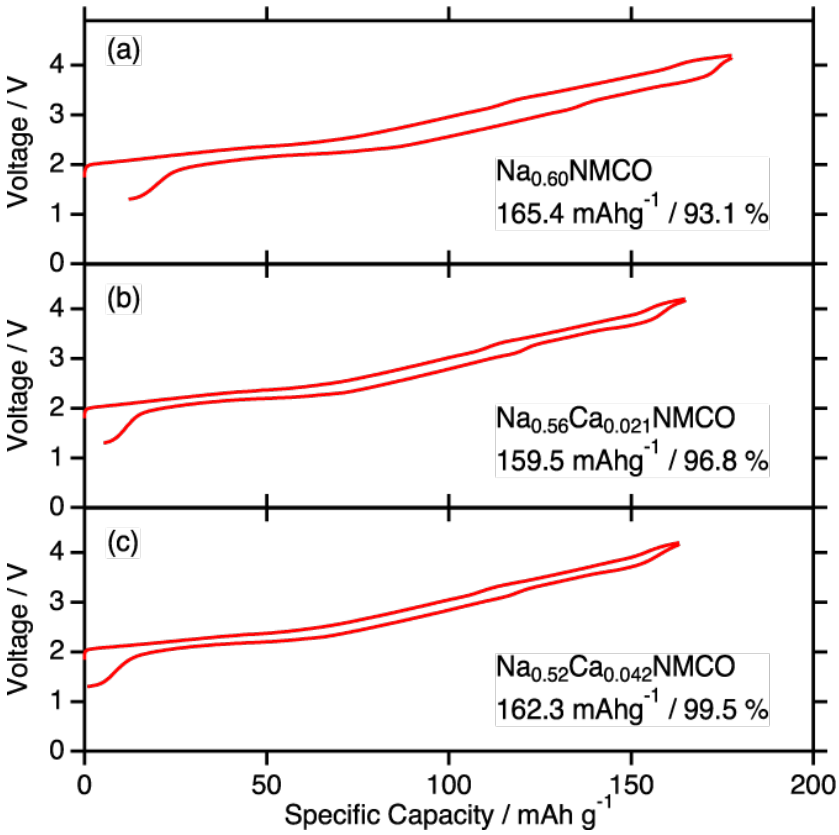

Figure. 2 Typical charge-discharge profiles of the P3-type $Na_{0.6}$NMCO (a), $Na_{0.56}Ca_{0.02}$NMCO (b) and $Na_{0.52}Ca_{0.04}$NMCO (c) in the voltage range of 1.3-4.2 V.

We also performed the charge-discharge test of the $Na_{0.6-2x}Ca_{2x}$NMCO (x=0, 0.04) at the charge cut-off voltage of 4.5 V, as shown in Figure 3. Another plateau appeared > 4.35 V expands the charging capacity up to 227.2 mAhg^{-1}. However, the NNMCO shows the discharging capacity of 195.5 mAhg^{-1}; consequently, the coulombic efficiency drops to 86.0 %. In addition, the voltage drops of 0.1 V between the end of the charge and the beginning of the discharge profile, indicate the irreversible reaction of the NNMCO at the high voltage region.

On the other hand, Figure 3 (b) shows that the Ca–substituted $Na_{0.52}Ca_{0.04}$NMCO maintains high coulombic efficiency of 95.2 %, even at the high cut-off voltage and the charge and discharge capacity between 4.5 V and 1.3

V are 196.8 and 187.4 $mAhg^{-1}$, respectively. We suspect the irreversible capacity of $Na_{0.52}Ca_{0.04}NMCO$ observed at high voltage is mainly due to the decomposition of the electrolyte solution. Figure S3 shows a linear sweep voltammogram (LSV) of the electrolyte solution using a Pt thin film electrode. The oxidation of the electrolyte solution gradually occurs > 4.0 V, and the peak current is observed at 4.53 V. Therefore, both the phase transition of the layered cathode active materials and the decomposition of the electrolyte solution cause the irreversible capacity during the charge-discharge process at the high cell voltage > 4.0 V.

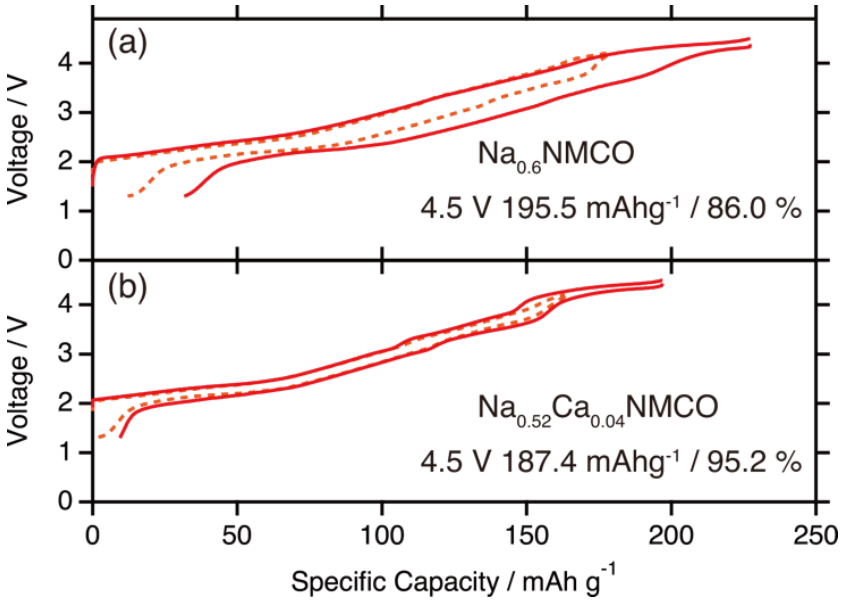

Figure. 3 Charge-discharge profiles of the P3-type $Na_{0.6}NMCO$ (a) and $Na_{0.52}Ca_{0.04}NMCO$ (b) in the voltage range of 1.3-4.5 V (solid line) and 1.3-4.2 V (dashed line)

In order to understand the phase transition process upon the Na^+ ion insertion/extraction, the phase stabilities of the NNMCO and NCNMCO are investigated by ex-situ XRD. The XRD patterns of the $Na_{0.60}NMCO$ and $Na_{0.52}Ca_{0.04}NMCO$ during the initial charge-discharge process are shown in Figure 4. The $Na_{0.60}NMCO$ maintained the hexagonal P3 phase with R-3m or R3m space group up to 4.3 V. The slight broadening of the 105 peak at 46 º indicates the formation of the monoclinic P'3 phase, as shown in Figure 4 (a). Once the electrode is charged up to 4.4 V, the diffraction pattern of the NNMCO significantly changed. A new peak appeared at 43 º is indexed to 104 peak of the O3' phase. Figure 4 (a) also shows the peak splitting of the 003 peak at 4.4 V during the charging process. The peak splitting suggests the intergrowth of the O3' phase with the P3 phase. The P3-O3' phase transition at high voltage is similar to the $Na_xFe_{1/2}Co_{1/2}O_2$[18], and $Na_x(Mn_{0.25}Fe_{0.25}Co_{0.25}Ni_{0.25})O_2$ system[29], reported in the past.

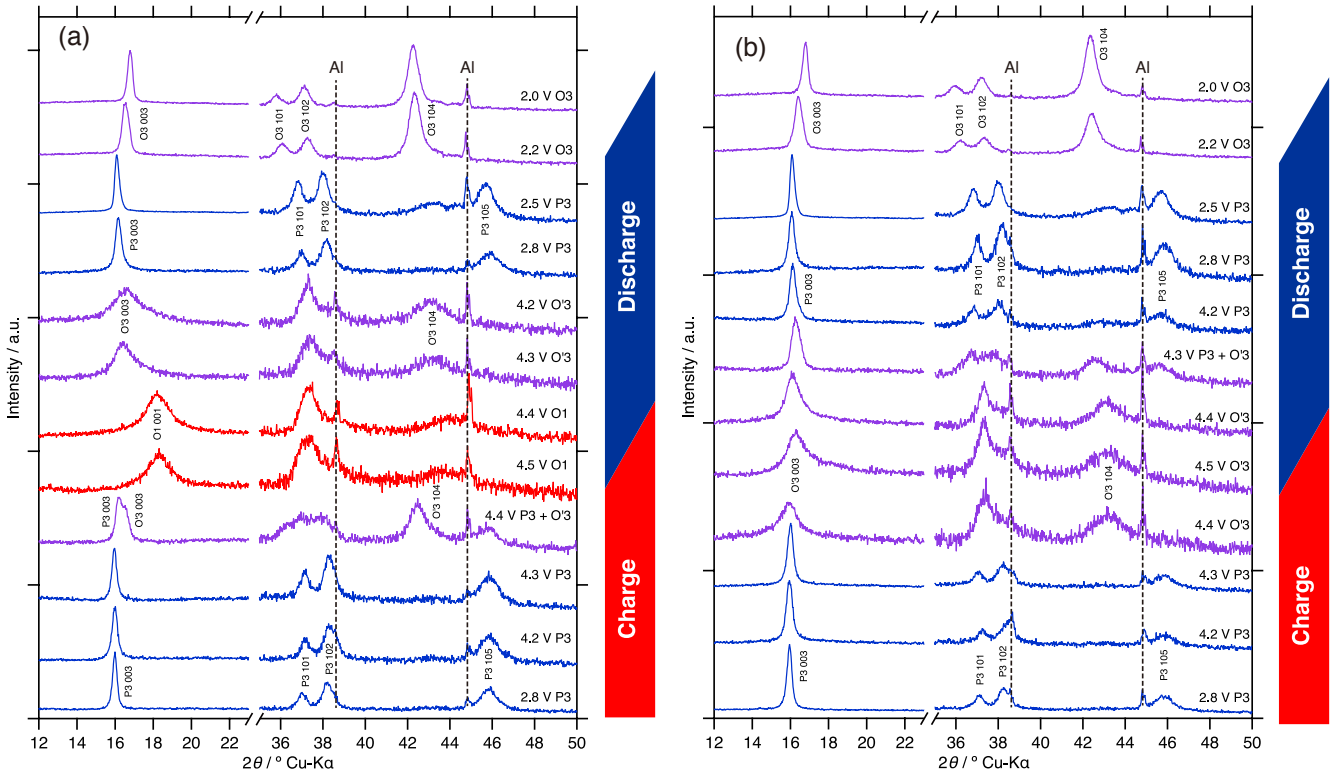

Figure. 4 Ex-situ X-ray diffraction patterns of P3-type $Na_{0.6}$NMCO (a) and $Na_{0.52}Ca_{0.04}$NMCO (b) during the charge-discharge process. The whole patterns are shown in Figure S4.

Subsequently a large peak shift of the 003 peak to higher angle with significant peak broadening at 4.5 V is observed. The peak shift corresponds to another phase transition to the O1 phase, as shown in the XRD pattern of the NNMCO upon the full Na^+ ion extraction[36, 37]. The peak broadening is probably due to the stacking faults between the slabs because the crystallinity of the NNMCO recovers after the discharging to < 2.8 V. The O1 phase is maintained even at 4.4 V during the discharging process. We suspect that the Na^+ de-intercalation is not completed at 4.4 V during the initial charging process due to the decomposition of the electrolyte solution, as we discussed in the previous section. The poor crystallinity of the O1 phase remains even after the phase transition to O3' phase at 4.2 V. Therefore, the stacking faults are considered to disappear during the O3'–P3 phase transition process. The further discharging leads the NNMCO to transform to the O3' phase at 2.2 V. The formation of the O3' phase at high Na content is a typical phase transition behavior of O3-P3 type layered materials.

The NCNMCO shows slightly different phase stability upon charge-discharge process as shown in Figure 4 (b). The P3 phase of the NCNMCO instead shows slight lattice shrinkage along the c-axis, associated with the deintercalation of Na^+ ions. The NCNMCO also observes the P3–O3' phase transition at 4.4 V with loss of the

crystallinity. On the other hand, the 003 peak of the O'3-type NCNMCO does not shift to higher 2θ, suggesting that the phase transformation to O1 phase does not occur even at 4.5 V. We guess that the remaining Ca^{2+} ions prevent the lattice shrinkage along the c-axis. The reformation of the P3 phase during the discharging process takes place at 4.3 V, while the NNMCO still shows the O3' phase even at 4.2 V. The crystallinity of the NCNMCO recovers at 4.3 V, indicating that the Ca^{2+} ions effectively stabilize the P3 phase. The slight shift of the 003 peaks, through the charge-discharge process, proves the Ca^{2+} ion substitution prevents the O3'-O1 phase transition at high electrode potential >4.3.

We performed Galvanostatic cycling tests for the NNMCO or NCNMCO/Na half-cells, as shown in Figure 5. At first, the cells were operated at 10 mAg^{-1} for the initial three cycles. Subsequently, the current was increased to 200 mAg^{-1} for the following 100 cycles. Then the additional two cycles at 10 mAg^{-1} were carried out again for the confirmation of the recovery of the capacity at low current density.

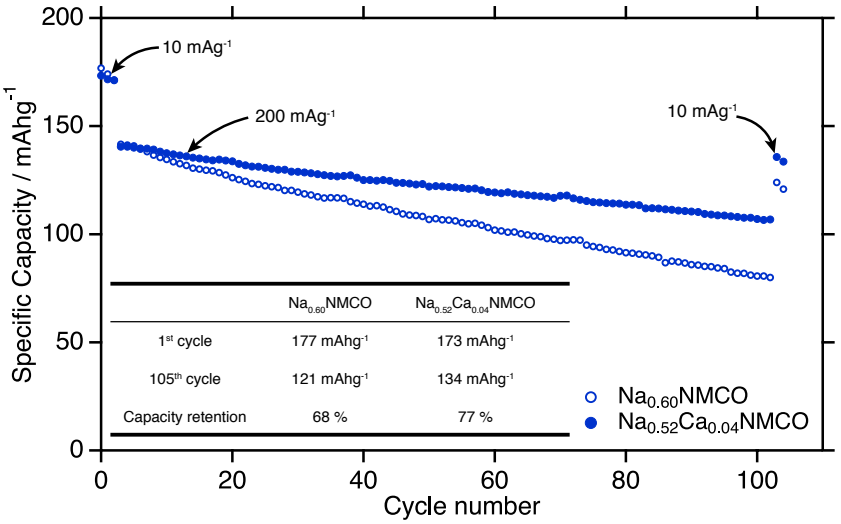

Figure. 5 Cycling performance of P3-type $Na_{0.6}NMCO$ and $Na_{0.52}Ca_{0.04}NMCO$. The galvanostatic cycling was performed at the current density of 200 mA g^{-1} and the voltage range of 2.5-4.2 V.

The NCNMCO/Na half-cell, of course, shows improved cycling performance, compared with the NNMCO due to the suppressed irreversible phase transition. The capacity retention of the NCNMCO after the 105 cycles is approximately 75 % while the NNMCO shows the capacity retention of 68 %. Notably, NCNMCO shows the capacity retention of 76 % during high-rate cycling. On the other hand, NNMCO shows capacity retention of 56 %. We suspect the fast capacity decay is due to the slow kinetics of the phase transition upon Na insertion/extraction. Therefore, the capacity significantly recovers during the last two cycles at the low charge-discharge rate.

Figure 6 compares the XRD patterns of the NNMCO and the NCNMCO electrodes at 4.2 V after the initial discharging process and the cycling test for 105 cycles. Both the NNMCO and NCNMCO show the P3 phase

after the initial charge-discharge process, as we already discussed in the previous section. The NCNMCO also maintains the P3 phase even after the cycling test. The slightly higher background around 2θ of 42–44 º indicates that the O'3 phase is partially formed. The 105 reflection peak at 46 º still proves the P3 phase is still stable even after the cycling test.

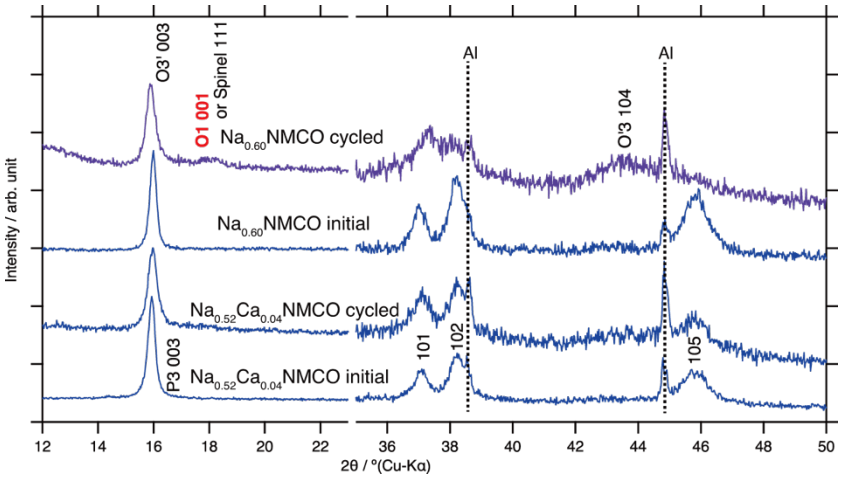

Figure. 6 XRD patterns of P3-type $Na_{0.6}$NMCO and $Na_{0.52}Ca_{0.04}$NMCO before and after the cycling test for 100 cycles at 200 mAg^{-1}.

On the other hand, the O3' phase is observed in the cycled NNMCO electrode. The XRD pattern of the cycled NNMCO also has a broad peak corresponding to 001 reflection of the O1 phase or the 111 reflection of unknown spinel phase: even the galvanostatic cycling test is carried out between 4.2 V and 1.3 V. We also speculate the high current density initiates an excess Na^+ extraction from the layered structure. The O1 phase is partially formed during the high-rate charging process. However, since the lattice constant of the O1 phase is significantly smaller than the O3' phase, we suppose the O3'-O1 phase transition is not desirably reversible and easily initiates the phase separation. Once the O1 phase is formed, we speculate the transition metal ions move to the tetrahedral or octahedral site in the Na layer, resulting in the spinel phase formation. The low crystallinity of the O1 or the spinel phase also indicates that the ionic/electronic conduction path is broken during the cycling test. Further microstructural analyses are necessary to confirm how the by-product remains in the structure during the deterioration process of the electrode.

We also performed SEM-EDX observation to confirm the distribution of Ca^{2+} ions in the layered material. Figure S7 shows SEM images and elemental mapping of the NCNMC composite electrode before/after cycling test. The uniform distribution of calcium shows that the Ca^{2+} ions are incorporated in the layered structure and never been extracted during the charge-discharge process. The non-extractable Ca^{2+} ions also indicate that the mobility of the Ca^{2+} ions is negligible. Thus, we conclude that the doped Ca^{2+} ions suppress the irreversible phase transition, resulting in the improved cycling performance.

As we previously reported, the P2-type Na_xCoO_2 shows improved cycling performance by the Ca^{2+} ion substitution. Hence the P3 type NCNMCO is also supposed to show improvement in cycling performance, as we discussed in the previous section. On the other hand, the loss of the specific capacity and the poor rate capability remain as predictable trades-off properties. The P3 type NCNMCO, however, shows better rate capability than we anticipated, as shown in Figure 7. The initial specific capacity of the NCNMCO is 162 $mAhg^{-1}$, while NNMCO shows the specific capacity of 177 $mAhg^{-1}$ at the specific current of 10 mAg^{-1} (approx. C/20). Once the specific current reaches to 400 mAg^{-1} (2C), both the NCNMCO and NNMCO show the capacity of 133 $mAhg^{-1}$. The NCNMCO shows higher capacity than NNMCO at 800 mAg^{-1} and 1600 mAg^{-1}. The higher capacity of the NCNMCO is not due to the capacity fading of the NNMCO, because the recovered capacity at the low current of 10 mAg^{-1} is still higher than the NCNMCO. The better rate capability of the NCNMCO is attributed to the enhanced Na^+ ion mobility in the expanded lattice by the Ca^{2+} ion substitution. In order to understand the excellent rate capability of the NCNMCO, we also conducted electrochemical impedance spectroscopy measurements during galvanostatic cycling. After the 10th and 70th cycle, the electrochemical impedance spectroscopy (EIS) measurements were carried out at various cell voltages. Figure 8 shows the Nyquist plots of the EIS for the NNMCO and the NCNMCO half-cells at 2.3, 3.2 and 4.2 V during the galvanostatic cycles. All the EIS spectra have two semicircles, the 1st one at high frequency region ($f \geq 100$ Hz) is corresponding to the Na^+ ion conduction in the porous electrode including the resistance of the SEI layer at the surface of the sodium metal anode. The 2nd one at low frequency region is corresponding to the charge-transfer resistance of the NNMCO and the NCNMCO.

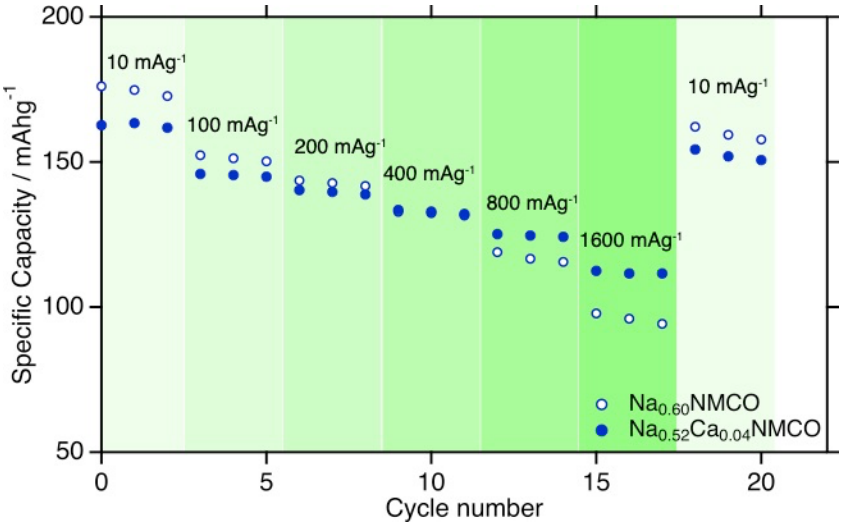

Figure. 7 Comparison of the rate capability of P3-type $Na_{0.6}NMCO$ and $Na_{0.6-2x}Ca_{0.04}NMCO$.

Even though the substituted Ca^{2+} ions are supposed to hinder the migration of the Na^+ ions, the charge-transfer resistance of the NCNMCO is rather lower than NNMCO < 3.3 V. The overall trend of the charge-transfer resistance and the electrode potentials is shown in Figure 8 (d). The reversible capacities of $Na_{0.6}NMCO$ and

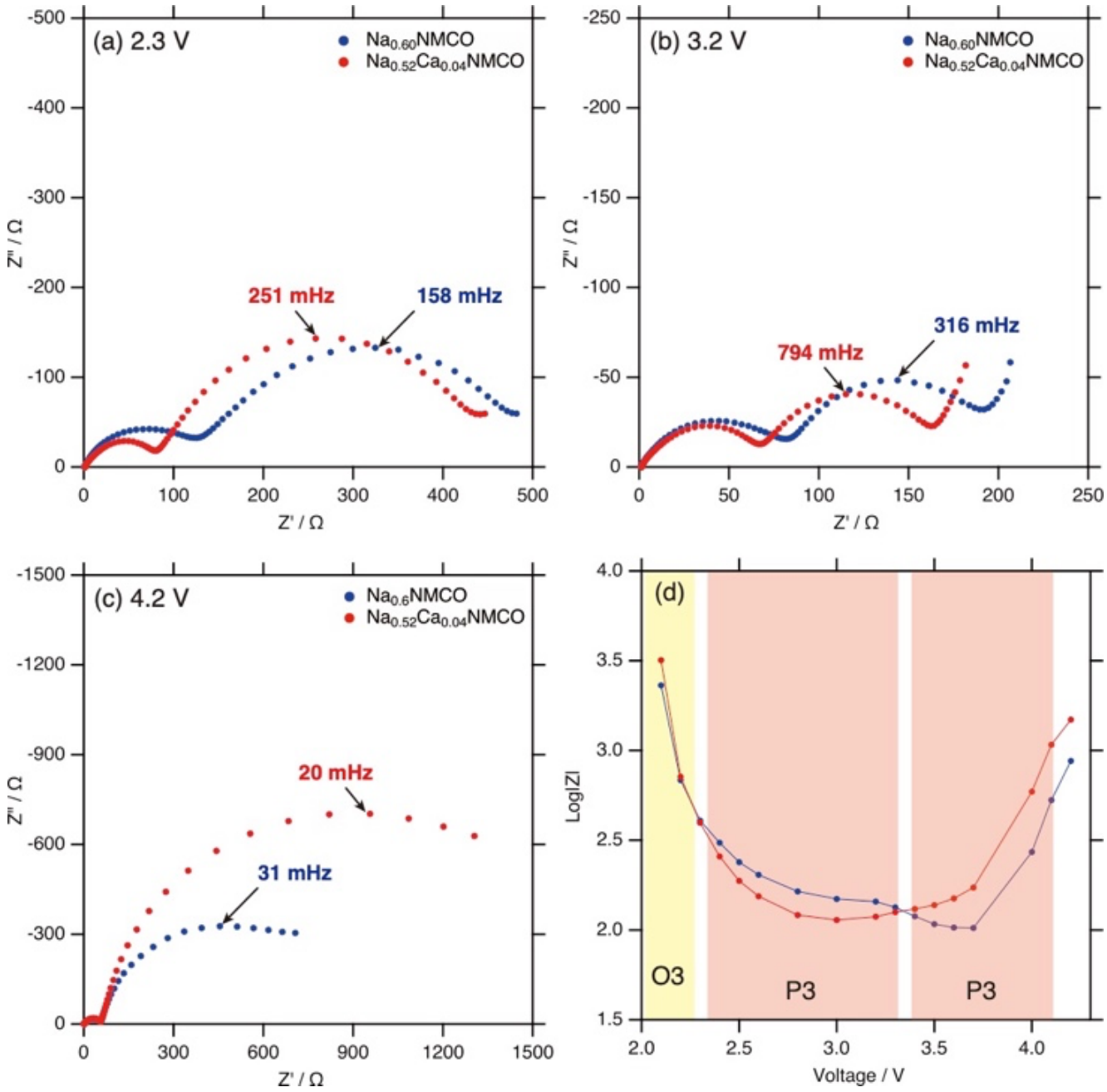

Figure. 8 Nyquist plots of the electrochemical impedance spectroscopies for P3-type $Na_{0.6}NMCO$ and $Na_{0.6-2x}Ca_{0.04}NMCO$ at 2.3 V (a), 3.2 V (b) and 4.2 V (c). The Ca^{2+} ion substation reduces the charge-transfer resistance at low voltage range (d).

$Na_{0.52}Ca_{0.04}NMCO$ <3.3 V are 140 $mAhg^{-1}$ and 123 $mAhg^{-1}$ respectively. Since the reversible capacity at the low voltage range corresponds to > 75% of the specific capacity obtained at 4.2-1.3 V, the Ca-substitution suppresses the cell resistance in most of the charge-discharge state. The voltage range is also in good agreement with the P3 single phase region of the NNMCO, reported by Sathiya et al. Furthermore, the Ca-substitution introduces more Na vacancies, consequently, the stable region of P3 phase expands to lower electrode potential. Even though the

Ca^{2+} ions hinder the migration of Na^{+} ions, we speculate that the expanded P3 region contributes to the improved mobility of the Na^{+} ions because activation energy of the mobile ions at the octahedral site is usually higher than the prismatic site.

As we already discussed above, the substituted Ca^{2+} ions have relatively strong electrostatic repulsion against the transition metal ions in the face-shared MeO_6 octahedra. On the other hand, the CaO_6 octahedron in the O3 phase has only the edge-shared MeO_6 octahedra. We expect no specific electrostatic repulsion force against the transition metal ions in the O3 phase. Therefore, we consider the lattice expansion in the P3 phase is the preferable factor that explains the improved rate capability of the NCNMCO. The cation vacancies formed by Ca^{2+} substitution in the Na^{+} ion layer also contribute to the improvement in mobilities of the Na^{+} ions. Furthermore, since the redox couple of the P3 single phase region in NNMCO is mainly corresponding to the Co^{3+}/Co^{4+}, we assume that the suppression of the charge-transfer resistance is also related to the electronic structure change. Further structural/electronic analyses are necessary to understand the origin of the lower charge-transfer resistance by the Ca^{2+} ion substitution.

CONCLUSION

In the present work, we successfully prove that the Ca^{2+} substitution of the P3-type layered $Na_xNi_{1/3}Mn_{1/3}Co_{1/3}O_2$ suppresses the O3'-O1 phase transition, which induces the capacity fading of the layered cathode. Even though the substituted Ca^{2+} ions, which are supposed to occupy the Na^{+} sites, the reversible capacity is maintained without increasing the overpotential, typically observed in the case of P2-type layered oxides. The structural analyses indicated that the electrostatic repulsion between the Ca^{2+} ion and the transition metal ion at the face-shared MO_6 site expands the lattice constant along the c-axis. The expanded sodium-layer accelerates the diffusion of sodium ions. We believe the concept of the materials design leads to overcome the trade-off of the overpotential and phase stability in the development of high voltage cathode active materials.

ASSOCIATED CONTENT

Supporting Information

The Supporting Information is available free of charge on the ACS Publications website.

AUTHOR INFORMATION

Corresponding Author

* E-mail: matsui@godzilla.kobe-u.ac.jp

Author Contributions

MM planned the research. FM, MM and HH carried out the experimental work. FM and MM analyzed the structural data. HH, NI and MM analyzed the electrochemical data. MM wrote the manuscript.

Funding Sources

This study was granted by Elements Strategy Initiative for Catalyst and Batteries of MEXT, Grant Number JPMXP0112101003. KAKENHI of MEXT Grant Number 18K19131 and 19H05813.

Notes

The authors declare no competing financial interest.

ACKNOWLEDGMENT

This study was partially supported by Elements Strategy Initiative for Catalyst and Batteries of MEXT, Grant Number JPMXP0112101003, KAKENHI of MEXT Grant Number 18K19131 and 19H05813. We also acknowledge Prof. Yasuo Takeda and Prof. Yasuaki Matsuda for helpful discussion.

Graphical abstract

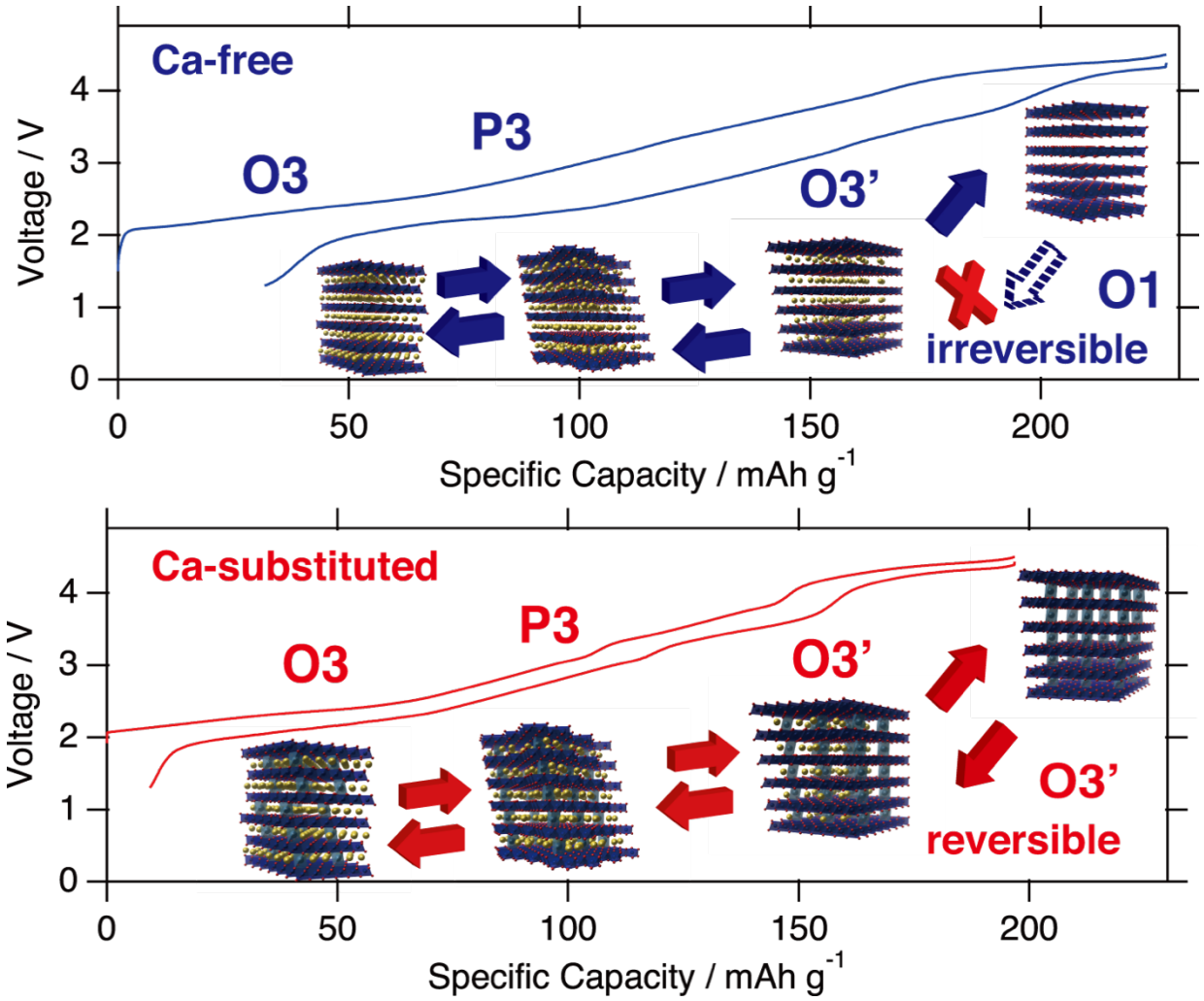

References

[1] N. Yabuuchi, K. Kubota, M. Dahbi, S. Komaba, Chem Rev, 114 (2014) 11636-11682.

[2] C. Delmas, C. Fouassier, P. Hagenmuller, Physica B, 99 (1980) 81-85.

[3] J.J. Braconnier, C. Delmas, P. Hagenmuller, Materials Research Bulletin, 17 (1982) 993-1000.

[4] A. Maazaz, C. Delmas, P. Hagenmuller, Journal of Inclusion Phenomena, 1 (1983) 45-51.

[5] A. Mendiboure, C. Delmas, P. Hagenmuller, Journal of Solid State Chemistry, 57 (1985) 323-331.

[6] S. Kikkawa, S. Miyazaki, M. Koizumi, Journal of Power Sources, 14 (1985) 231-234.

[7] Y. Takeda, K. Nakahara, M. Nishijima, N. Imanishi, O. Yamamoto, M. Takano, R. Kanno, Materials Research Bulletin, 29 (1994) 659-666.

[8] S. Komaba, C. Takei, T. Nakayama, A. Ogata, N. Yabuuchi, Electrochemistry Communications, 12 (2010) 355-358.

[9] D. Hamani, M. Ati, J.-M. Tarascon, P. Rozier, Electrochemistry Communications, 13 (2011) 938-941.

[10] X. Ma, H. Chen, G. Ceder, Journal of The Electrochemical Society, 158 (2011) A1307.

[11] R. Berthelot, D. Carlier, C. Delmas, Nat Mater, 10 (2011) 74-80.

[12] C. Didier, M. Guignard, C. Denage, O. Szajwaj, S. Ito, I. Saadoune, J. Darriet, C. Delmas, Electrochemical and Solid-State Letters, 14 (2011) A75.

[13] P. Vassilaras, X. Ma, X. Li, G. Ceder, Journal of The Electrochemical Society, 160 (2012) A207-A211.

[14] X. Xia, J.R. Dahn, Electrochemical and Solid-State Letters, 15 (2012) A1.

[15] X. Xia, J.R. Dahn, Journal of The Electrochemical Society, 159 (2012) A647.

[16] M. Guignard, C. Didier, J. Darriet, P. Bordet, E. Elkaïm, C. Delmas, Nature Materials, 12 (2013) 74-80.

[17] N. Yabuuchi, H. Yoshida, S. Komaba, Electrochemistry, 80 (2012) 716-719.

[18] H. Yoshida, N. Yabuuchi, S. Komaba, Electrochemistry Communications, 34 (2013) 60-63.

[19] I. Saadoune, A. Maazaz, M. Ménétrier, C. Delmas, Journal of Solid State Chemistry, 122 (1996) 111-117.

[20] J.M. Paulsen, J.R. Dahn, Solid State Ionics, 126 (1999) 3-24.

[21] S. Komaba, N. Yabuuchi, T. Nakayama, A. Ogata, T. Ishikawa, I. Nakai, Inorganic chemistry, 51 (2012) 6211-6220.

[22] N. Yabuuchi, M. Kajiyama, J. Iwatate, H. Nishikawa, S. Hitomi, R. Okuyama, R. Usui, Y. Yamada, S. Komaba, Nat Mater, 11 (2012) 512-517.

[23] D. Kim, E. Lee, M. Slater, W. Lu, S. Rood, C.S. Johnson, Electrochemistry Communications, 18 (2012) 66-69.

[24] X. Wang, M. Tamaru, M. Okubo, A. Yamada, The Journal of Physical Chemistry C, 117 (2013) 15545-15551.

[25] B. Mortemard de Boisse, D. Carlier, M. Guignard, L. Bourgeois, C. Delmas, Inorganic chemistry, 53 (2014) 11197-11205.

[26] B. Mortemard de Boisse, J.H. Cheng, D. Carlier, M. Guignard, C.J. Pan, S. Bordère, D. Filimonov, C. Drathen, E. Suard, B.J. Hwang, A. Wattiaux, C. Delmas, Journal of Materials Chemistry A, 3 (2015) 10976-10989.

[27] N. Yabuuchi, M. Yano, H. Yoshida, S. Kuze, S. Komaba, Journal of The Electrochemical Society, 160 (2013) A3131-A3137.

[28] G. Singh, F. Aguesse, L. Otaegui, E. Goikolea, E. Gonzalo, J. Segalini, T. Rojo, Journal of Power Sources, 273 (2015) 333-339.

[29] X. Li, D. Wu, Y.-N. Zhou, L. Liu, X.-Q. Yang, G. Ceder, Electrochemistry Communications, 49 (2014) 51-54.

[30] M. Sathiya, K. Hemalatha, K. Ramesha, J.M. Tarascon, A.S. Prakash, Chemistry of Materials, 24 (2012) 1846-1853.

[31] J.-Y. Hwang, C.S. Yoon, I. Belharouak, Y.-K. Sun, Journal of Materials Chemistry A, 4 (2016) 17952-17959.

[32] M. Matsui, F. Mizukoshi, N. Imanishi, Journal of Power Sources, 280 (2015) 205-209.

[33] Y. Ishado, H. Hasegawa, S. Okada, M. Mizuhata, H. Maki, M. Matsui, Chemical Communications, 56 (2020) 8107-8110.

[34] L. Sun, Y. Xie, X.-Z. Liao, H. Wang, G. Tan, Z. Chen, Y. Ren, J. Gim, W. Tang, Y.-S. He, K. Amine, Z.-F. Ma, Small, 14 (2018) 1704523.

[35] K. Momma, F. Izumi, Journal of Applied Crystallography, 44 (2011) 1272-1276.

[36] J.L. Kaufman, A. Van der Ven, Phys Rev Mater, 3 (2019).

[37] X.Q. Yang, X. Sun, J. McBreen, Electrochemistry Communications, 2 (2000) 100-103.